High Energy Physics Laboratory,
Department of Physics,
Nara Women's University,
Nara 630-8263, JAPAN

NWU-HEP 99-01

Development of the CsI(Tℓ) Calorimeter for the Measurement of CP Violation at KEK B-Factory

Hitomi Ikeda

Human Life and Environmental Science Course,
Graduate School of Human Culture,
Nara Women's University
Nara 630-8263, JAPAN

January 1999

Ph.D Dissertation

Abstract

The understanding of the origin of the CP violation is one of the most important subjects in recent particle and high energy physics. In order to make an systematic study of the CP violation in the B meson system, the BELLE detector was constructed.

We completed the construction of the electromagnetic calorimeter in December 1998, which is one of the most important part of the BELLE detector. We put our best foot forward the design and the test of its performance, since we need a precise calorimeter for the energy measurement of electrons and γ's.

The calorimeter consists of 8,736 pieces of 30 cm long thallium doped cesium iodide (CsI(Tℓ)) crystals and we did the energy calibration of each crystal by using cosmic rays before the installation.

The beam test was carried out using a photon beam in the energy range of 20 MeV to 5.4 GeV at the Budker Institute of Nuclear Physics (BINP), Russia. The calorimeter system has been tested in almost the same configuration as the BELLE experiment. The energy equivalent noise is $\sim$200 keV for one counter. The measured energy resolution is 4 % at 20 MeV and 1.7 % at 5.4 GeV for 5×5 matrix with a threshold of 0.5 MeV. This is better than any other similar detectors constructed, or being constructed in the world. The energy linearity is -3 ± 2 % for whole energy region. This is the first measurement of the linearity for such a wide energy range with the photon beam.

In analyzing the beam test data, we established an analysis method to obtain a best energy resolution. It helps us to detect the electron, γ and π^0 with good efficiency. We checked the expected detection efficiency for γ's and π^0's from $B\bar{B}$ decays by the GEANT simulation.

Contents

1 Introduction **1**

2 B Physics **5**

2.1 Motivation of B Physics 5

2.1.1 CP Violation 5

2.1.2 CKM Matrix 8

2.1.3 B-factory 11

2.2 Indirect CP Violation 12

2.3 Direct CP Violation 16

3 KEKB Accelerator and BELLE Detector **17**

3.1 KEKB Accelerator 17

3.2 BELLE Detector 18

3.2.1 Overall Design 18

3.2.2 Beam Pipe 21

3.2.3 Silicon Vertex Detector(SVD) 21

3.2.4 Extreme Forward Calorimeter(EFC) 24

3.2.5 Central Drift Chamber(CDC) 24

3.2.6 Aerogel Čerenkov Counter(ACC) 25

3.2.7 Time of Flight Counter(TOF) 25

3.2.8 Electromagnetic Calorimeter(CsI) 25

3.2.9 Super Conducting Magnet 28

3.2.10 K_L and Muon Detector(KLM) 28

3.2.11 Trigger and DAQ System 28

4 CsI(Tℓ) Calorimeter **30**

4.1 Introduction 30

4.2 Principle of Calorimetry 32

4.3 Crystal Calorimeter 36
4.3.1 Energy Resolution 36
4.3.2 Position Resolution 38
4.3.3 Detection Efficiency 38
4.3.4 Choice of Crystal 39
4.4 Layout of the BELLE Calorimeter 39
4.4.1 Overall Arrangement 39
4.4.2 Shape of the Crystals 42
4.5 CsI(Tℓ) Crystal 44
4.5.1 Production 44
4.5.2 Light Output and Uniformity 45
4.5.3 Size Measurement of the CsI(Tℓ) Crystal. 47
4.5.4 Radiation Hardness 50
4.6 CsI(Tℓ) Counter Module 50
4.7 Mechanical Structure 54
4.8 Readout Electronics 57
4.8.1 Overall Design 57
4.8.2 Photodiode 59
4.8.3 Preamplifier 61
4.8.4 Shaper/QT 61
4.8.5 Time to Digital Converter (TDC) 63
4.8.6 Calibration Module 65
4.8.7 Trigger 66

5 Energy Calibration of CsI(Tℓ) Counters 72
5.1 Introduction 72
5.2 Setup 73
5.3 Analysis 75
5.4 Energy Scale 75
5.5 Light Output Result 79
5.6 Uniformity of Light Collection 81

6 Test of the CsI(Tℓ) Calorimeter Performance by Photon Beam. 84
6.1 Motivation 84
6.2 Photon Beam 84
6.3 Experimental Setup 87

6.4 Data Collection 90
6.5 Electronics Performance 92
6.5.1 Noise Level 92
6.5.2 Electronics Linearity 93
6.5.3 Electronics Calibration 95
6.6 Energy Calibration 96
6.7 Energy Resolution 102
6.7.1 Tagged Photon Analysis 102
6.7.2 Compton Edge 103
6.7.3 Bremsstrahlung Edge 103
6.7.4 Asymmetry Parameter 105
6.7.5 Energy Resolution for Simple Sum 105
6.7.6 Energy Resolution with Threshold 108
6.7.7 Comparison with Monte Carlo Simulation 109
6.7.8 Error in Resolution 118
6.8 Energy Linearity 120
6.8.1 Compton Edge and Bremsstrahlung Edge 120
6.8.2 Comparison with Monte Carlo Simulation 120
6.8.3 Discussion 123
6.9 Summary and Conclusion 130

7 Expected Performance **131**
7.1 Simulation of γ and π^0 Detection 131
7.1.1 BELLE Simulation 131
7.1.2 γ Detection 132
7.1.3 π^0 Mass Resolution 135
7.1.4 Selection of π^0 137
7.1.5 π^0 Detection Efficiency 138
7.1.6 S/N Ratio 139
7.1.7 Summary 140

8 Conclusion **141**

A Chronicles of CsI(Tℓ) Crystal Production for BELLE **147**

B CsI(Tℓ) Crystal Size **153**

C Compton Fitting Function **165**

Chapter 1

Introduction

The goal of the particle physics is to understand the nature by searching the ultimate constituent elements of matter and to explain the forces responsible for the interactions among them. We have a standard model[1],[2],[3], for the explanation of their forces. The standard model is the theory that six types of quarks; up(u), down(d), strange(s), charm(c), bottom(b), top(t) and six types of leptons; electron(e), muon(μ), tau(τ), and neutrinos(ν_e, ν_μ, ν_τ) interact through the agency of gauge particles; photons(γ) mediate the electromagnetic force, Z^0 and $W^\pm$ bosons mediate the weak forces and gluons(g) mediate the strong forces.

Prediction of the standard model has good agreements with the experimental results until 100 GeV, but many issues still await settlement. One of the most important issue is the origin of CP violation. The CP violation is believed to relates on the basic principle of the nature. For example, if we believe that the universe was born with the same amount of matter and anti-matter as explained in the Big-Ban model[4], the CP violation is a key issue to explain why the universe we live in consists predominantly of the matter.

Although the CP violation was first observed 35 years ago in the K meson system, we still do not understand how it occurs. In 1973, Kobayashi and Maskawa[5] noted that, with three quark generations, the CP violation could be accommodated in the standard model. In the KM model, the CP violation is caused by the imaginary phase of the rotation matrix of three generations of quarks. This is an elegant and economical manner of the explanation. We do not know, however, whether this explanation is quantitatively correct.

The magnitude of the CP violating asymmetry in the K meson system is in the order of 10^{-3}. It was pointed out that the CP violation in certain decay modes of B

mesons will be much bigger than that in K mesons. The CP violating asymmetry in the B mesons is expected to be an order of $\sim 10\%$ [6],[7],[8]. In addition to the magnitude of the CP asymmetry, the B meson system is also an ideal place for systematic studies of the KM matrix elements, since experimental results can be related to the theory more directly than that in the case of the K mesons, thanks for the large mass value of the bottom quark.

The observation of the CP asymmetry in B meson system, thus, is an important milestone to the full understanding of the mystery of the CP violation in the nature. For this purpose. the B factory project was initiated 5 years ago [9],[10] at the High Energy Accelerator Research Organization(KEK) in Tsukuba, Japan. The importance of this research is reflected in the number of competitors to this project. The SLAC-B[11],[12] project in USA and the HERA-B[13] project in Germany also started at almost the same time and all three projects are planning to start their experiments in 1999.

In order to measure the CP violation in the B meson system, several advanced techniques are required both for accelerator and detector components. The KEKB accelerator is under construction in the same TRISTAN tunnel to generate a large amount of B mesons. It is the colliding accelerator which has 2 rings. Electrons and positrons are accelerated with different energies (asymmetric accelerator) in order to detect the decay vertex of the B mesons. The center of mass energy is just set on the mass of the $\Upsilon(4S)$ state (10.580GeV), where a pair of B and $\bar{B}$ mesons is produced. The accelerator is designed to achieve the luminosity $10^{34}\mathrm{cm}^{-2}\mathrm{s}^{-1}$, which is 2 orders of magnitude larger than those of any existing e^+e^- machines.

In the interaction point of the KEKB accelerator, a large detector with high performance, BELLE is located. The construction of the detector itself is also the challenging task. It should be emphasized that the typical branching fraction of the decay modes of B which have a large CP asymmetry, is in the order of 10^{-4} to 10^{-5}. Therefore B mesons in this small branching fraction should be reconstructed exclusively by keeping backgrounds as low as possible. This requirement leads that the detector system should have highest possible resolutions and efficiencies in each subdetector component. We need precise tracking devices for momentum measurements of charged particles, precise calorimeters for energy measurements of electrons and photons, precise vertex detectors for the determination of decay vertices of the B mesons. The identification of leptons

(electron, muon), kaons, pions as well as K_L^0's is also required. And all of them should be integrated in one detector system.

I devoted 5 years of my life to study of the design and the construction of the BELLE electromagnetic calorimeter which is one of the most important parts of the BELLE detector. The calorimeter consists of 8,736 of 30 cm long, thallium doped, cesium iodide (CsI(Tℓ)) crystals. The function of the calorimeter is to measure the total energy of photons and electrons by detecting all activities in the electromagnetic showers in the calorimeter material. The reconstruction of π^0 (and η^0) mesons is the most important function of the BELLE calorimeter, since about one third of the decay products of B mesons include π^0 mesons and π^0 decays to two photons(γ). The calorimeter should cover a wide range of energies from 20 MeV to 8 GeV with a good energy resolution. The electrons (or positrons) can be identified by using informations of the calorimeter and the tracking device. An electron carries an important information to determine their mother particles as either B^0 or $\bar{B}^0$ mesons (B tagging). The tagging of the B mesons is essential for the measurement of the CP violation.

This thesis is a collection of all my works, which includes the design of the calorimeter in the early stage, the construction of the actual calorimeter and the test of the detector performance. The thesis is organized as follows:

- Physics motivations and theoretical backgrounds of the B-factory project are described in chapter 2.
- Overview of the KEKB accelerator and the BELLE detector are given in chapter 3.
- Design principles and the detailed design of the BELLE electromagnetic calorimeters are described in chapter 4. The description includes the design of each counter, the supporting system of crystals and the readout electronics. The results of R&D works which were done in the design stage are also described.
- Calibration of 8,736 crystals on crystal by crystal basis is the most elaborating and important work in the construction of the calorimeter. This has been carried out by using cosmic rays. The method and the system of the calibration with cosmic ray and the results are described in chapter 5.
- Results of the beam test, which was carried out using a tagged photon facility at the Budker Institute of Nuclear Physics (BINP), Russia, are presented in chapter

6. In this beam test, the calorimeter system has been tested in almost the same configuration of the real experiment. To our knowledge, the resolution shown here is better than any other similar detectors ever constructed, or being constructed all over the world. The linearity of the energy response is also checked in the ranges from 20 MeV to 5.4 GeV. This is the first measurement of the linearity for such a wide energy range with the photon beam. This chapter describes an important milestone of my work in the BELLE collaboration.

- Expected performance of the electromagnetic calorimeter in the BELLE detector is discussed based on the Monte Carlo simulations in chapter 7.

- The thesis is concluded in chapter 8.

The calorimeter was installed to the BELLE detector in September to December, 1998. All other detector components were successfully integrated into BELLE by the end of December 1998. We are now making a fine tuning of each subdetector by using cosmic rays.

A brief history of the construction of the calorimeter is summarized in appendix A. Although it is impossible to write all details in this thesis, the reader can see from this history how the calorimeter has been constructed. We met several serious troubles in the construction of the BELLE calorimeter, which is the biggest crystal calorimeter to date. Fortunately those problems were overcome and we completed the construction.

The physics experiment is expected to start in spring, 1999, a few months later from now.

Chapter 2

B Physics

2.1 Motivation of B Physics

2.1.1 CP Violation

One of the most important concepts in physics is the symmetry or invariance under the operation in space and time. The symmetry strongly relates to the conservation laws. The conservation laws limit the possible interactions. For example, a momentum is conserved under the translation in space and an angular momentum is conserved under the rotation in space. These are the examples of the continuous transformation.

On the other hand, discrete transformation include a charge conjugation C, a space reflection P and a time reversal T. The transformation of physical observables under the C, P and T operation is summarized in Table. 2.1.

The operation of the spatial reflection on the wave function $\Psi(\mathbf{r})$ is produced by the operator P, where

$$P\Psi(\mathbf{r}) \to \Psi(-\mathbf{r}). \tag{2.1}$$

A repetition of this operation gives;

$$P^2\Psi(\mathbf{r}) \to P\Psi(-\mathbf{r}), \tag{2.2}$$

$$P^2\Psi(\mathbf{r}) \to \Psi(\mathbf{r}), \tag{2.3}$$

$$P^2 = 1. \tag{2.4}$$

		transformation		
		C	P	T
coordinate	$\mathbf{r}$	$\mathbf{r}$	$-\mathbf{r}$	$\mathbf{r}$
momentum	$\mathbf{p}$	$\mathbf{p}$	$-\mathbf{p}$	$-\mathbf{p}$
angular momentum	$\mathbf{J}$	$\mathbf{J}$	$\mathbf{J}$	$-\mathbf{J}$
spin	σ	σ	σ	$-\sigma$
electric field	$\mathbf{E}$	$-\mathbf{E}$	$-\mathbf{E}$	$\mathbf{E}$
magnetic field	$\mathbf{B}$	$-\mathbf{B}$	$\mathbf{B}$	$-\mathbf{B}$
particle		antiparticle	particle	particle

Table 2.1: C, P, T transformation of physical observables.

We obtain the eigen value or the parity $P = \pm 1$ for the space reflection. The parity is a multiplicative number, then if $\Psi = \phi_1\phi_2 \cdots$, the parity is equal to the product of the parity of each part and $(-1)^l$ where l is the orbital angular momentum of the particles in the system.

The charge conjugation C reverses the sign of the charge and the magnetic moment of a particle. The C transformation means the interchange of a particle and an antiparticle. The T transformation replaces the time T with $-$t and makes the time to flow in opposite direction. All three discrete transformations C, P and T have their own eigen value (parity) $\pm$ 1.

The violation of the space reflection symmetry in the weak interaction (P violation) predicted by Lee and Yang [14] and was found by Wu *et al.* in ^{60}Co β decay (^{60}Co (J=5) $\rightarrow {}^{60}Ni^*$ (J=4) $+ e^-\ \bar{\nu}_e$) in 1957[15]. A high proportion of ^{60}Co nuclei spin was aligned at $0.01°K$. The relative electron intensities along and against the field direction were measured in the magnet. The polarization of ^{60}Co was determined from the angular distribution of γ's from ^{60}Co. The results for the electron intensity distribution is described;

$$I(\theta) = 1 + \alpha(\frac{\sigma\mathbf{p}}{E}) = 1 + \alpha\frac{v}{c}cos\theta, \tag{2.5}$$

where $\alpha = -1$, σ is a unit spin vector, $\mathbf{p}$ and E are the electron momentum and total energy, θ is the angle of emission of the electron. The observed asymmetry of (2.5) signified the P violation.

The weak interactions also violates the charge conjugation invariance. An exam-

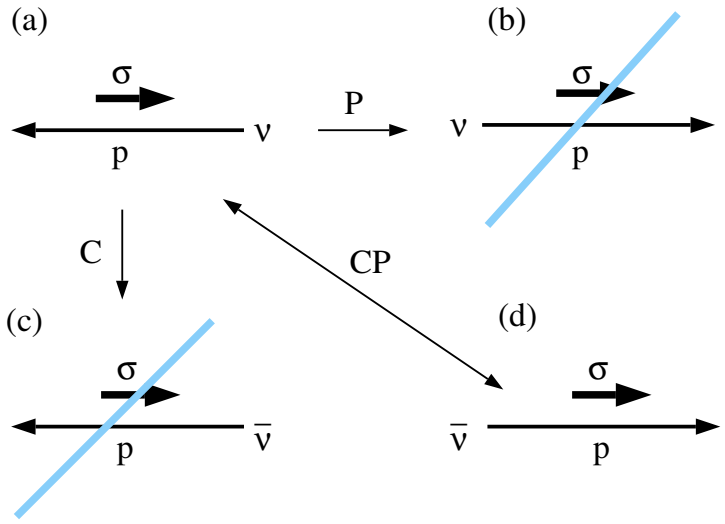

Figure 2.1: Results of C and P transformation on neutrino states. Only (a) and (d) are observed in neutrinos.

ple is a neutrino state. As shown in Fig. 2.1, neutrinos are 'left-handed'[16] and anti-neutrinos are 'right-handed'. But right-handed neutrinos and left-handed anti-neutrinos don't exist. It means that the weak interactions are not invariant under C and P transformation separately, but the CP invariance seems to be held.

The CP violation was first observed in K^0 system in 1964[17]. The K^0 particle decays by weak interaction into two pions of $CP = 1$ or three pions of $CP = -1$. The two pion decay has a decay time $\sim 9 \times 10^{-11}$ s and three pion decay has $\sim 5 \times 10^{-8}$ s. We may assume that the K^0 and $\bar{K^0}$ are composed of two particles K_1 and K_2, and each decays to two and three pions conserving the CP invariance;

$$|K^0 > \equiv \frac{|K_1 > + |K_2 >}{\sqrt{2}}, \tag{2.6}$$

$$|\bar{K^0} > \equiv \frac{|K_1 > - |K_2 >}{\sqrt{2}}, \tag{2.7}$$

where the CP of K_1 and K_2 is defined as follows;

$$CP|K_1 >= +|K_1 >, \tag{2.8}$$
$$(C = -1, P = -1, CP = +1),$$

$$CP|K_2 >= -|K_2 >, \tag{2.9}$$

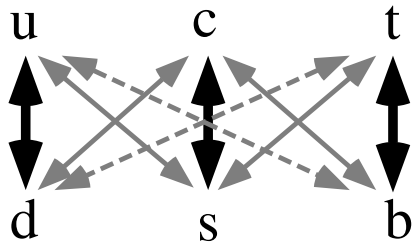

Figure 2.2: Weak transition of quarks.

$$(C = +1, P = -1, CP = -1).$$

If the CP invariance exists, K_1 should decay into two pions and K_2 should decay into three pions. But it was observed that K_2 decayed into two pions with the probability of 2×10^{-3}. This means the physical eigenstates K_S^0 and K_L^0 defined by their mass and decay time are different from the weak eigen states K^0 and $\bar{K^0}$. And they can be expressed by K_1 and K_2 as;

$$|K_S^0 >= |K_1 > +\varepsilon|K_2 >, \tag{2.10}$$

$$|K_L^0 >= |K_2 > +\varepsilon|K_1 >, \tag{2.11}$$

where $\varepsilon \neq 0$ signifies the CP violation. The origin of the CP violation is not at present established. The CP violation of K_0 is very small and was observed only in the K_0 and $\bar{K_0}$ system.

2.1.2 CKM Matrix

In the Standard Model (SM) of elementary particles, quarks interact with $W^{\pm}$ and Z^0 bosons and change in the flavor charge current weak interaction (see Fig. 2.2).

The interaction Lagrangian of this process is given by;

$$L_{int} = \frac{g}{\sqrt{2}} \left\{ (\overline{u}, \overline{c}, \overline{t})_L \gamma^{\mu} W_{\mu}^{+} \mathbf{V} \begin{pmatrix} d \\ s \\ b \end{pmatrix}_L + \left(\overline{d}, \overline{s}, \overline{b}\right)_L \gamma^{\mu} W_{\mu}^{-} \mathbf{V}^{\dagger} \begin{pmatrix} u \\ c \\ t \end{pmatrix}_{\mathbf{L}} \right\}, \tag{2.12}$$

g : coupling constant
$(\ )_L$: left handed quarks
γ^{μ} : γ matrix
$W_{\mu}^{\pm}$: $W^{\pm}$ boson

where $\mathbf{V}$ is a 3×3 unitary matrix called Cabbibo-Kobayashi-Maskawa (CKM) matrix. Kobayashi and Maskawa pointed out that the CP violation can be explained as a complex phase of the matrix $\mathbf{V}$ and it can be accommodated only if more than or equal to three pairs of quark flavors exist [5]. The Wolfenstein parameterization for the matrix is [18]

$$\mathbf{V} \equiv \begin{pmatrix} V_{ud} & V_{us} & V_{ub} \\ V_{cd} & V_{cs} & V_{cb} \\ V_{td} & V_{ts} & V_{tb} \end{pmatrix} = \begin{pmatrix} 1-\frac{\lambda^2}{2} & \lambda & A\lambda^3(\rho - i\eta) \\ -\lambda & 1-\frac{\lambda^2}{2} & A\lambda^2 \\ A\lambda^3(1-\rho-i\eta) & -A\lambda^2 & 1 \end{pmatrix} + O(\lambda^4). \tag{2.13}$$

The CKM matrix includes four parameters λ, A, ρ and η which have to be determined by experiments. As described below, the values λ and A are well constrained but the value of ρ and η are not determined well.

The free parameter λ is the sine of the Cabbibo angle $\sin\theta_c$ [20], and is well determined from strange particle decays such as $K \to \pi l^+ \nu$ [21], $\Sigma \to ne\bar{\nu}$ [22], nuclear β decay [23], and the production of the charm quark in ν interactions $\nu + d(s) \to \mu^- + c$, $\bar{\nu} + \bar{d}(\bar{s}) \to \mu^+ + \bar{c}$ [24] to be

$$\lambda = 0.221 \pm 0.002. \tag{2.14}$$

V_{cb} is determined from the measurement of the branching ratio for the decay $\bar{B}^0 \to D^+ \ell^- \bar{\nu}$, $\bar{B}^0 \to D^{*+} \ell^- \bar{\nu}$ and inclusive semileptonic decay $\bar{B}^0 \to X\ \ell^- \bar{\nu}$. The average value of V_{cb} is 0.0381 ± 0.0021, which gives the value of A to be [25]

$$A = 0.784 \pm 0.043. \tag{2.15}$$

The value of V_{ub} was obtained from both the exclusive and the inclusive analysis of the charmless b decay; $B \to \rho l \nu$ [26][27] and $B \to X_u l \nu$ [28]. The measurement of the parameter V_{ub} provides a constraint

$$(\frac{1}{\lambda^2})|\frac{V_{ub}}{V_{cb}}|^2 = (\rho^2 + \eta^2) = (0.36 \pm 0.07)^2. \tag{2.16}$$

Neutral B mesons can transform to their anti-particles before they decay. We will discuss the phenomenon of the $B - \bar{B}$ mixing in section 2.2. The probability of mixing is given by [29] [30] [31] [32] [33] [34].

$$x \equiv \frac{\Delta m}{\Gamma} = \frac{G_F^2}{6\pi^2} B_B f_B^2 m_B \tau_B |V_{tb}^* V_{td}|^2 m_t^2 F(\frac{m_t^2}{M_W^2}) \eta_{QCD}, \tag{2.17}$$

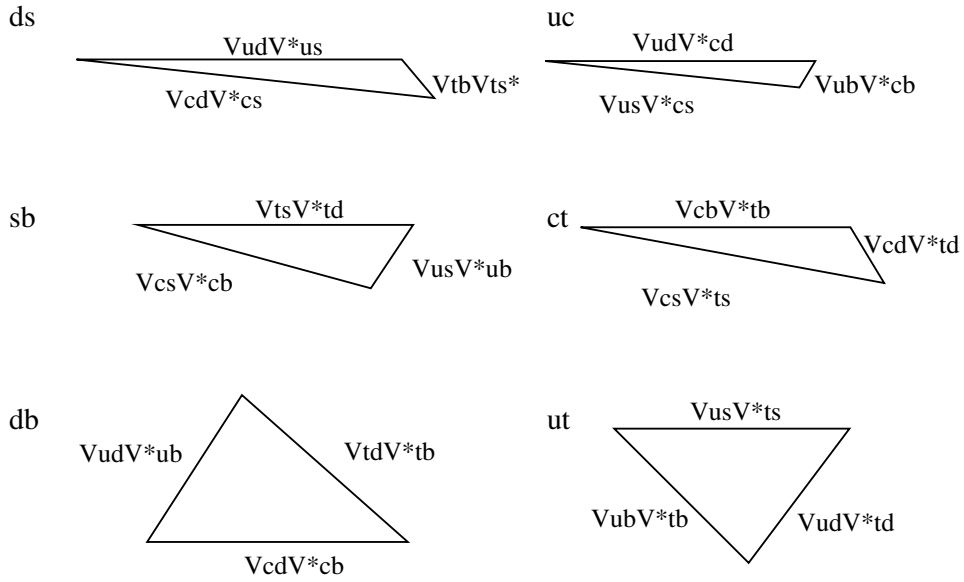

Figure 2.3: Six unitarity triangles following from the orthogonality of the CKM matrix.

where 'bag parameter' B_B is a parameter related to the probability of the d and $\bar{b}$ quarks forming a hadron, f_B is the decay constant, F is a known function which increases approximately as m_t^2 and η_{QCD} is a QCD correction with value about 0.8. Since

$$|V_{tb}^* V_{td}|^2 \propto |(1-\rho-i\eta)|^2 = (\rho-1)^2+\eta^2, \tag{2.18}$$

the value of x gives a constraint in the $\rho-\eta$ plane. There is also a constraint on ρ and η given by the K_L^0 CP violation measurement (ϵ), given by

$$\eta((1-\rho)A^2(1.4\pm0.2)+0.35)A^2\frac{B_K}{0.75} = (0.30\pm0.06). \tag{2.19}$$

The limit of $K^0 \to \pi\pi$ decay (ϵ') can be translated to limits on η given by [35],

$$Re(\epsilon/\epsilon') = (0.19\pm0.09)\times10^{-2}A^2\eta(1-0.46(\frac{m_t}{100GeV/c^2}-0.7)^2). \tag{2.20}$$

The theoretical constraint on the CKM matrix comes from the unitarity of the matrix as follows;

$$\mathbf{V}^\dagger\mathbf{V} = \begin{pmatrix} V_{ud}^* & V_{cd}^* & V_{td}^* \\ V_{us}^* & V_{cs}^* & V_{ts}^* \\ V_{ub}^* & V_{cb}^* & V_{tb}^* \end{pmatrix}\begin{pmatrix} V_{ud} & V_{us} & V_{ub} \\ V_{cd} & V_{cs} & V_{cb} \\ V_{td} & V_{ts} & V_{tb} \end{pmatrix} = I. \tag{2.21}$$

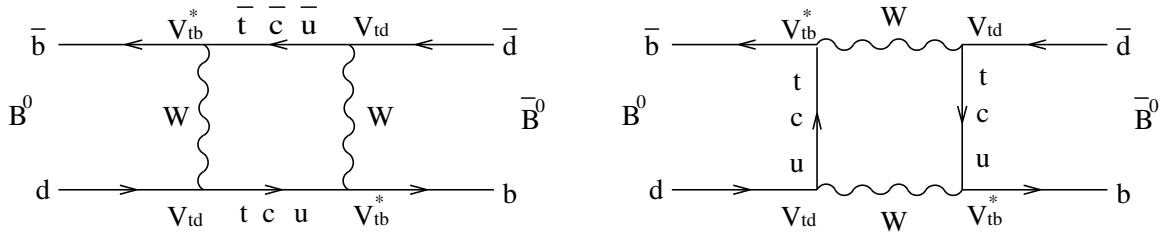

Figure 2.4: Feynman diagram of $B\bar{B}$ mixing.

The condition $\sum_i V_{ji}^* V_{ik} = \delta_{ij}$ gives 6 triangles in the complex plane as shown in Fig. 2.3. Each triangle is marked by a quark pair to which the triangle gives constraints on that transition. It is the flavor changing neutral current (FCNC) transitions between each quark pair. The direct (Born level) FCNC transition is forbidden in SM but it is possible through the box diagrams which is shown in Fig. 2.4. For example, (ds) triangle shows the constraint on the s $\rightarrow$ d transition which is observed in $K^0(\bar{K}^0)$ transition. By measuring three angles and three sides of the triangles, the CKM matrix elements can be determined with over constraint.

2.1.3 B-factory

The goal of the BELLE experiment is to perform definitive tests on the Kobayashi-Maskawa predictions for the CP violation in B meson decays [19]. This is related with the (db) triangle described by the following equation ;

$$V_{ud}V_{ub}^* + V_{cd}V_{cb}^* + V_{td}V_{tb}^* = 0. \tag{2.22}$$

The triangle shape which three sides are defined as $V_{td}V_{tb}^*$, $V_{ud}V_{ub}^*$ and $V_{cd}V_{cb}^*$ and three internal angles are defined as

$$\phi_1 \equiv arg(\frac{V_{cd}V_{cb}^*}{V_{td}V_{tb}^*}), \tag{2.23}$$

$$\phi_2 \equiv arg(\frac{V_{ud}V_{ub}^*}{V_{td}V_{tb}^*}), \tag{2.24}$$

$$\phi_3 \equiv arg(\frac{V_{cd}V_{cb}^*}{V_{ud}V_{ub}^*}). \tag{2.25}$$

The shape of the triangle is shown in Fig. 2.5 with the constraints for the CKM parameters.

The KEK B-factory is constructed for the measurement of three angles and three sides of this triangle. A large number of Υ(4S)'s are produced by KEKB collider

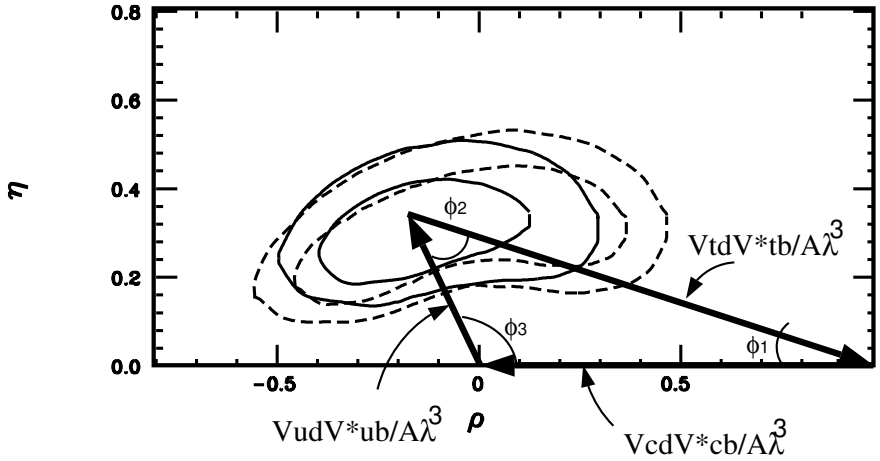

Figure 2.5: Allowed region in the $\rho - \eta$ plane estimated from presently available data. Solid curves : $|V_{cb}|$, $|V_{ub}|/|V_{cb}|$, ϵ, Re(ϵ'/ϵ), x_d and m_t as constraints; Dashed curves : without x_d and Re(ϵ'/ϵ). The inner (outer) curves denote 1σ (90% C.L.) regions.

through the collision of e^+e^- beams at the center of mass energy $\sqrt{S} = 10.58$ GeV. The Υ(4S) decays to a $B\bar{B}$ pair and specific decay modes of B will be reconstructed by the BELLE experiment. Various decay modes usefull for the determination of the side and the angle are tabulated in Table. 2.2.

2.2 Indirect CP Violation

When the B^0 and $\bar{B}^0$ mesons decay into the same CP; $B^0 \to f$ and $\bar{B}^0 \to f$, the CP violationg asymmetry A_f is given by

$$A_f = \frac{R(B^0 \to f) - R(\bar{B}^0 \to f)}{R(B^0 \to f) + R(\bar{B}^0 \to f)} = sin2\phi_{CP} sin(\Delta m \Delta t), \tag{2.26}$$

where Δm is the mass difference between two B^0's and Δt is the difference of proper time for B^0 and $\bar{B}^0$ decays. $R(B^0 \to f)$ is the decay rate of $B^0 \to f$.

The asymmetry is produced by the interference of two amplitudes (Fig. 2.4); a direct decay $B^0 \to f$ and a decay through the $B\bar{B}$ oscillation $B^0 \to \bar{B}^0 \to f$ which is called as the indirect CP violation. Experimentally the measurement of Δt is essential for the observation of the asymmetry. We can measure Δt using the Lorenz boost of the Υ(4S) state produced by the asymmetry of beam energies as described later. The angle ϕ_{CP} is the phase difference between two amplitudes, which is directly related to the internal angle of the unitarity triangle.

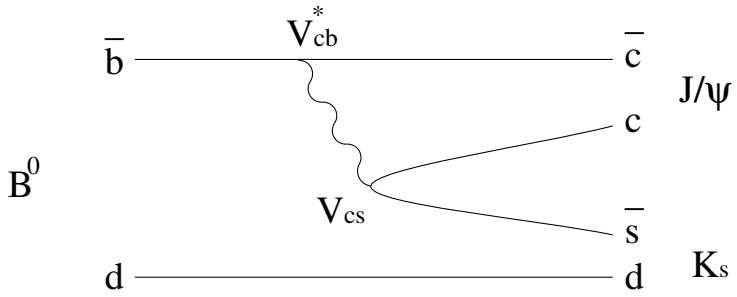

Figure 2.6: Feynman diagram for $B^0 \to J/\psi K_s^0$

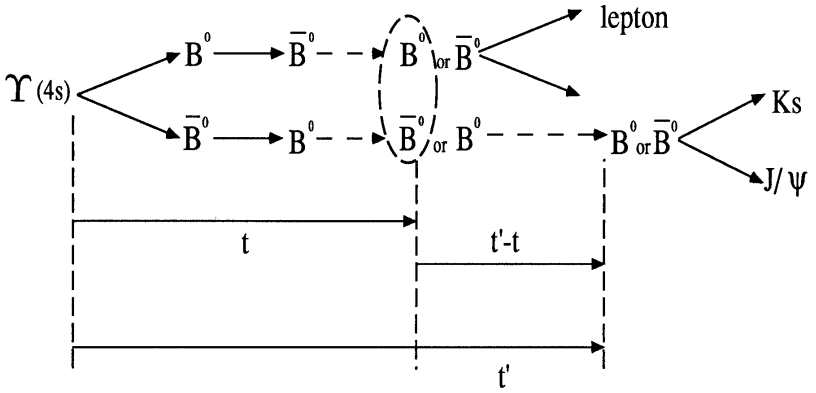

Figure 2.7: Measurement of time difference (t'-t) for $B^0 \to \mathrm{J}/\psi\ K_s$.

	λ^n	
ϕ_1	λ^2	$\eta_c K_s$ ψK_s $\psi' K_s$ $\psi'' K_s$ χK_s $\eta_c K^*$ $\eta_c K_s\pi^0$ $D_{1,2}\pi^0$ $D_{1,2}\omega$ $D_{1,2}\rho^0$ ψK^* $\psi' K^*$ $\psi'' K^*$ $\psi K_s\pi^0$ $\psi' K_s\pi^0$ $\psi'' K_s\pi^0$
	λ^3	$D^0\bar{D}^0$ D^+D^- D^*D D^0K_s $D^0K_s\pi^0$ $\eta_c\pi^+\pi^-$ $D^0\bar{D}^0\pi^0$ $D^+D^-\pi^0$ $\psi\pi^+\pi^-$ $\psi'\pi^+\pi^-$ $\psi''\pi^+\pi^-$ $D^*D\pi^0$
ϕ_2	λ^3	$\pi^+\pi^-$ $\pi^0\pi^0$ $\rho^0\pi^0$ $\omega\pi^0$ $\eta\pi^0$ $\pi^+\pi^-\pi^0$ $\eta\pi^+\pi^-$ $\eta\pi^0\pi^0$ $a_1^\pm\pi^\pm$ $\rho^\pm\pi^\mp$ $\rho^+\rho^-$ $\rho^0\rho^0$ $\rho^0\omega$ $\omega\omega$ $\rho^0\pi^0\pi^0$ $\rho^0\pi^+\pi^-$ $\omega\pi^+\pi^-$
	λ^4	$K^\pm\pi^-$
ϕ_3	λ^3	$B_s \to \rho K_s$ $B_s \to \phi K_s$ $B^0 \to K_s D^0$ $B^0 \to D^0 K_s\pi^0$ $B^\pm \to D^0 K^\pm$ $B^\pm \to D^0 K^\pm\pi^0$ $B^\pm \to D^0 K_s\pi^0$
$\lvert V_{ud}V_{ub}^*\rvert$		$B \to \rho\ell\nu$ $B \to \pi\ell\nu$
$\lvert V_{td}V_{tb}^*\rvert$		$B_d \leftrightarrow \overline{B}_d$,$B_s \leftrightarrow \overline{B}_s$ mixing
$\lvert V_{cd}V_{cb}^*\rvert$		$B \to D^*\ell\nu$

Table 2.2: Decay modes of B meson useful for the determination of unitarity triangle.

For example, a decay mode $B^0 \to J/\psi K_s^0$ (Fig. 2.6) can be used to measure the angle ϕ_1. The asymmetry in this decay is given by

$$\frac{R(B^0 \to J/\psi K_s^0) - R(\bar{B}^0 \to J/\psi K_s^0)}{R(B^0 \to J/\psi K_s^0) + R(\bar{B}^0 \to J/\psi K_s^0)} = sin2\phi_1 sin(\Delta m \Delta t). \tag{2.27}$$

A schematic view of the measurement is illustrated in Fig. 2.7. Since the $B\bar{B}$ pair produced from the Υ(4S) is a coherent state with $C = -$, when one of the pair decays as a B at the time t, the other one is determined as $\bar{B}$ at the same time. This phenomenon is a famous Einstein-Podolsky-Rosen's paradox. We know the flavor of the first decay at the time T from the lepton charge of the semileptonic decay as shown in Fig. 2.8. The flavor tagged $\bar{B}$ decays to $J/\psi K_s^0$ at the time t'. Then a nonzero value of A_f will be observed as the function of Δt = t' − t. The Monte Carlo simulation of the proper time for the expected asymmetry (sin2ϕ_1=0.6) is shown in Fig. 2.9.

The expected asymmetry ranges from 0.02 to 0.2 [36]. The CP asymmetry is observed with 3 σ significance if d × sin2ϕ_1 is larger than 0.37 with an integrated luminosity of 10 fb^{-1} [37] where d is a dilution factor.

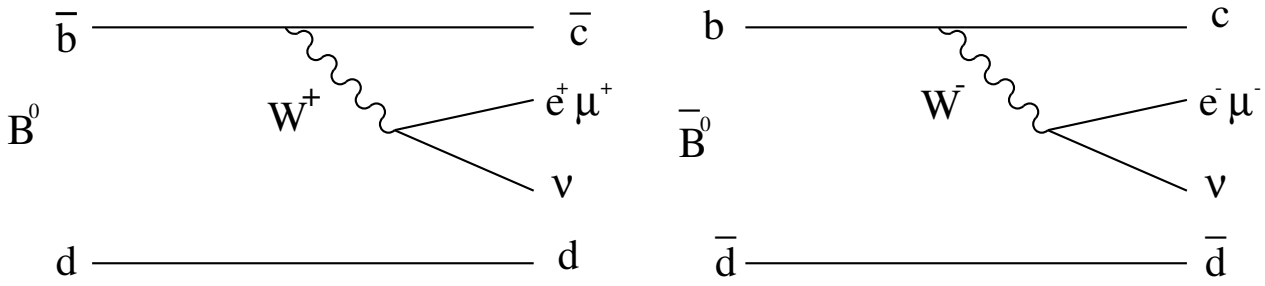

Figure 2.8: Feynman diagram for B tagging.

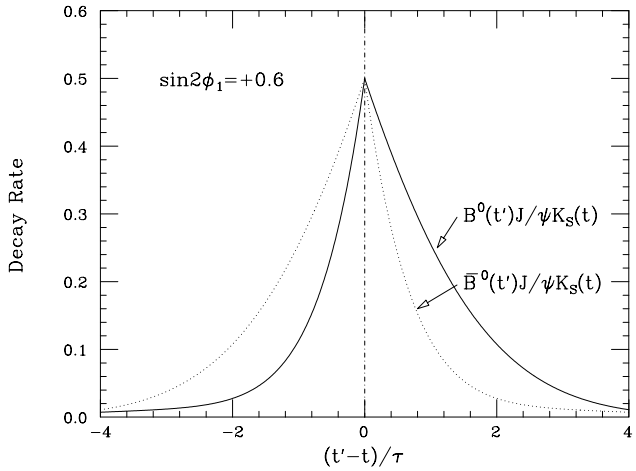

Figure 2.9: Proper time distribution of t'−t in $B \to J/\psi K_s^0$.

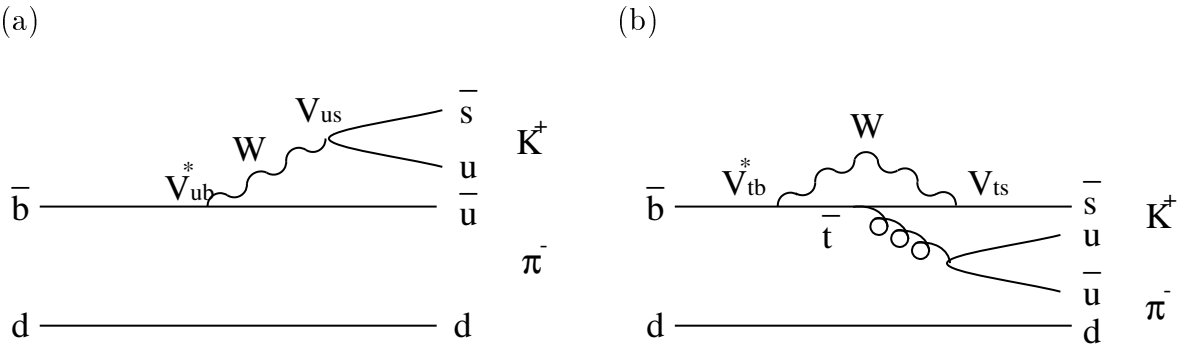

Figure 2.10: Feynman diagram for $B^0 \to K^+\pi^-$.(a)tree diagram and (b)penguin diagram.

2.3 Direct CP Violation

A direct CP violation means the difference between the decay rate of $B \to f$ and its charge conjugation decay rate of $\bar{B} \to \bar{f}$;

$$R(B \to f) \neq R(\bar{B} \to \bar{f}). \tag{2.28}$$

The direct CP violation occurs when there is an interference between two decay diagrams having different weak complex phases and different strong complex phases with the amplitudes of similar size. An example is shown in Fig. 2.10 for $B^0 \to K^{\pm}\pi^{\mp}$. In this decay mode, there are contributions from the tree and penguin diagrams and they have different phases.